Numerical Analysis of the Flow at the Tip of a High Pressure Turbine Blade when using Winglets

Pamela Martinez[1], Luis Moreno[1], Juan Barbosa[1]

[1](Postgraduate and Investigation Studies Section, National Polytechnic Institute, Mexico)
Corresponding Author: Pamela Martinez

Abstract: *A research about the application of winglets at the tip of a rotor blade of a high pressure turbine from the CFM56 engine applying computational fluid dynamics was made. Two geometries were analyzed, the first one applying a winglet at the leading edge and the suction surface, the other one with the winglet at the leading edge and the pressure surface. The results were compared with the ones obtained from the analysis of the original blade configuration, proving that by using winglets at the blade tip, the efficiency increases.*
Keywords: *Blades, high pressure turbine, stage efficiency, winglets.*

I. Introduction

In recent years multiple investigations with the aim of reducing aerodynamic losses and thermal stresses present in turbomachinery have been made, especially on the high pressure turbine blades. The reason is that these problems can cause a decrement of work and an increment in blades failures, diminishing the performance of the gas turbine.

The aerodynamic losses are generated due to the union of the flows with different velocities and pressures around the blade, creating different types of vortices. When the blade tip vortices interact with the principal flow, the development of vortices at the suction surface is encouraged, provoking that over 30% of total losses of the turbine are generated at the blade tip.

That is the reason why several researchers [1-3] have chosen this topic as their subject of investigation, proving that the tip geometry has an important role on the stage efficiency. These studies inspired the use of squealers [4], which reduce losses but are still not efficient enough. However, the use of winglets has been studied, obtaining very good results and increasing the stage efficiency.

The first time that the use of winglets at the tip of a turbine blade was proposed was in 1980, when Patel [5] showed that double winglets (winglets on both, suction and pressure surfaces) increase the efficiency by 1.2%. More recently, Dey and Camci [6] researched in 2001 the effect of winglet width variation in both, pressure and suction surfaces, proving that using winglets on the pressure surface does not affect the efficiency, contrary to the winglets used on the suction surface.

In 2013, Lee et al. [7] took care of finding the best width/pitch ratio, concluding that as this ratio increased, the vortices between the blades decreased but the tip vortices magnified. Nonetheless, they discovered that when this ratio had a value of 10.55%, the losses generated by the vortices between the blades diminished and the ones provoked by the tip vortices remained constant, turning this ratio the optimum.

Additionally, in 2016 Morales da Silva et al. [8] performed a numerical study of different high pressure turbine blade tips, measuring the pressure drop and the static pressure and temperature distribution, obtaining a greater efficiency by using winglets. Furthermore, it was concluded that altering the blade tip influences over the principal flow, making a more adequate study necessary.

Finally, Sarabia [9] determined in 2018 that by using winglets on the blade tip, the stage efficiency increases. Besides, he discovered that combining squealers and winglets had a negative effect on the blade performance.

That is why this investigation focused on analyzing the flow and the tip vortices when using winglets. In this case, two geometries were studied: the first one with winglets on leading edge and suction surface; the second, with winglets on leading edge and pressure surface.

The obtained results were compared with the ones from the analysis of the original blade, making it possible to visualize the flow variations by implementing winglets.

II. Winglets geometry

Due to the requirement of analyzing the complete high pressure turbine stage, it was necessary to obtain both, stator and rotor characteristics. The airfoils and the number of blades were acquired from the CFM56 engine manual [10].

The stator is constituted by 36 blades, with a height of 60 mm and a chord equal to 90 mm. The rotor counts with 85 blades and a tip clearance of 3 mm.

The first case (case A) is a rotor blade with winglet on the leading edge and the suction surface, with a winglet width equal to 5 mm along the entire geometry and a thickness of 1 mm. The second case (case B) is a rotor blade with winglet on the leading edge and the pressure surface, with the same characteristics as the one from case A. In Fig. 1 these geometries can be visualized.
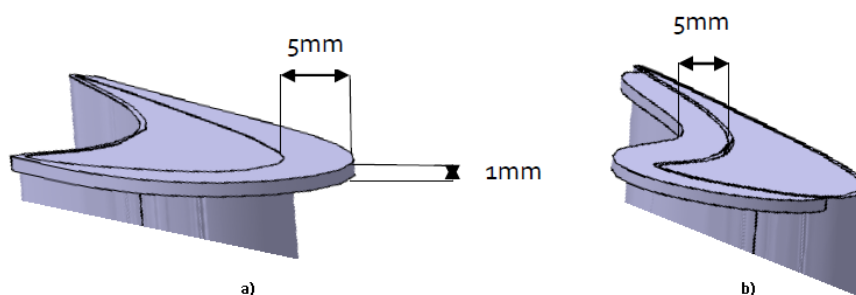

Figure 1. Winglet geometry from a) case A and b) case B.

III. Meshing

In order to mesh the entire geometry (stator and rotor) the module AutoGrid5^{TM} by NUMECA International was used, which generates high quality full automatic multi-block structured meshing [11]. For every case, a value of y$^+$ equal to 1 was considered and the mesh topology selected was HOH. It is important to mention that a butterfly meshing was utilized for the tip clearance.

3.1 Mesh independence

The mesh independence was performed with the blade from the base case, meaning the blade without winglets.

In Table 1 the characteristics of all the proposed meshes are listed, such as the number of grid points and the time spent on simulation.

Table 1. Obtained results from the mesh independence study.

Case	Difference of mass flow (%)	Number of grid points	Time of simulation
1	0.068	4909876	3.4 days
2	0.068	4206740	2.8 days
3	0.083	3786844	2.3 days
4	0.092	1856750	1.8 days

Thanks to the previous results, it was concluded that the most adequate mesh was the second one, because, should the first two cases are compared, less time of simulation was spent on the second one and the difference of mass flow remained constant.

1. CFD Analysis

The simulations were tridimensional in steady state using the module FINE/Turbo by NUMECA International. The selected turbulence model was Spalart Allmaras, due to Belmont and Talavera's investigation [12], who determined in 2016 that this model provided results similar to the ones from the experimental research.

The stablished boundary conditions at the inlet were the mass flow, equal to 83.2 kg/s, and the static temperature, with a magnitude of 1577.62 K. At the outlet, the considered boundary condition was the static pressure, equal to 564.970 kPa.

Regarding the initial conditions, they were determined based on the CFM56 engine operation parameters, which are listed in Table 2.

Table 2. CMF56 engine operation parameters.

Rotational speed	14324 rpm
Inlet temperature	1577.62 K
Outlet temperature	1380.8 K

Inlet pressure	2325.130 kPa
Outlet pressure	564.97 kPa
Blade tip velocity	400 m/s

IV. Results

The aerodynamic losses can be translated into pressure drop; therefore, static pressure and temperature losses analysis were performed in order to observe the pressure gradients, which cause the tip vortices. Relative velocity vectors, entropy and efficiency were also studied for each case.

In order to analyze the results correctly, the blade was separated into nine segments dependent on the chord, which are listed in Table 3.

Table 3. Blade segments dependent on the chord used for the results analysis.

Segment	% of chord	Distance from the trailing edge
1	0%	0 mm
2	10.6%	5 mm
3	20%	10 mm
4	30%	15 mm
5	40%	20 mm
6	55%	26 mm
7	70%	34 mm
8	80%	39 mm
9	100%	47 mm

5.1 Static pressure at the blade channel

In the base case, it was possible to visualize that at 30% of the chord the flow separation at the suction surface and the tip clearance started. It was also seen that at 40% of the chord the leakage vortices started to form, completing its generation at 55% of the chord at the suction surface. Furthermore, at 70% of the chord at the pressure surface the tip clearance losses started to be present, increasing until joining with the suction surface at 80% of the chord.

In the case A, at 30% of the chord a decrement of the separation at the suction surface was visualized. Additionally, there was no formation of low pressure zones at the tip clearance, which started to form until the 70% of the chord, where also, at the suction surface, the leakage vortex started to generate, which means a delay in the separation of the flow. However, the greatest difference was that in this case, at the trailing edge, a decrease of low pressure zones took place, which diminishes the leakage vortices and efficiency losses.

5.2 Relative velocity vectors

In the base case, at 55% of the chord at the suction surface a recirculation zone exists, which can be seen in Fig. 2a. At 70% of the chord, the leakage vortex started to form, Fig. 2b, being far more evident at 80% of the chord, Fig. 2c, where the formation of the vortex and the difference in velocity at the tip clearance can be visualized, having a relative velocity equal to 1000 m/s at the tip clearance and equal to 600 m/s around the suction surface, generating a recirculation, as can be seen in Fig. 2d.
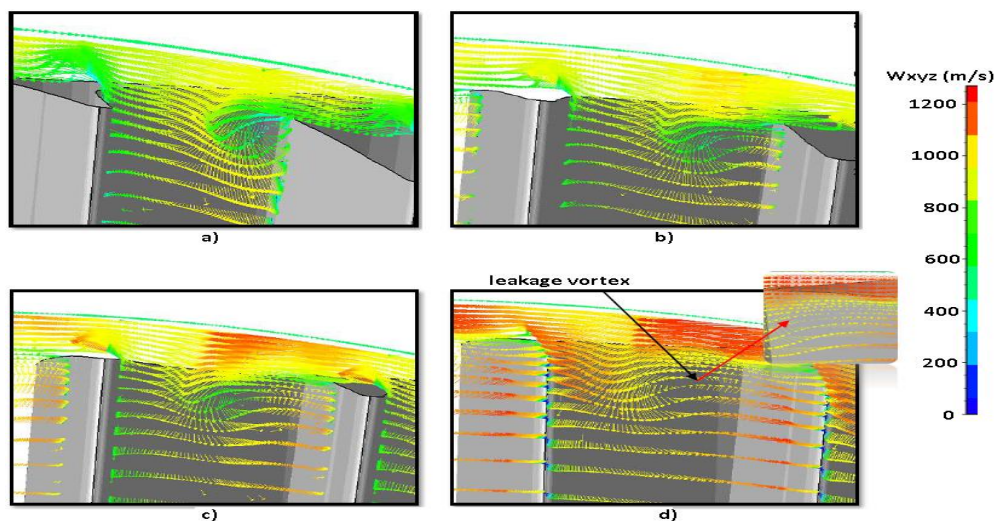

Figure 2. Relative velocity vectors from base case at a) 55% of the chord, b) 70% of the chord, c) 80% of the chord and d) trailing edge.

The situation changes in case A, where at 40% of the chord a recirculation of velocity vectors at the tip clearance at the suction surface could be distinguished, which generated a delay in the separation of the flow that can be identified at 55% of the chord in Fig. 3a. Continuing with the comparison, at 70% of the chord a decrement of the difference in velocities between the tip clearance and the blade channel exists, as can be observed in Fig. 2b, which avoided the complete formation of leakage vortices. Additionally, at 80% of the chord, Fig. 3c, and at the trailing edge, Fig. 3d, can be visualized that the implementation of winglets generated a dissipation and decrement of the leakage vortex intensity, increasing the stage efficiency.

Now, comparing the case B with the base case, the differences become evident at 70% of the chord, Fig. 4b, where the leakage vortex generation started at the suction surface, but with the variation that this vortex is displaced towards the suction surface, which interrupts the vortex development without affecting the formation of the leakage vortex. Its formation can be identified at the trailing edge, Fig. 4d, although with a smaller intensity than the one in the base case.
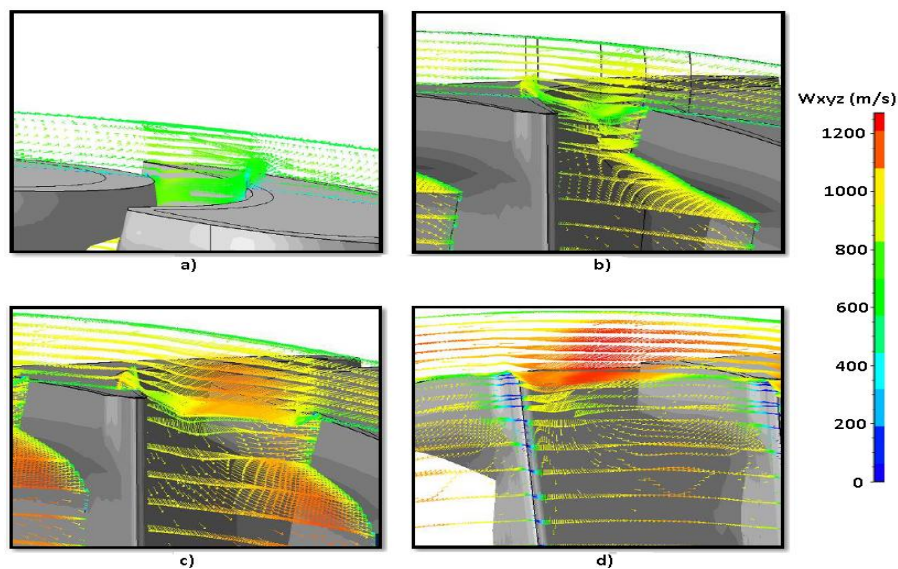

Figure 3. Relative velocity vectors from case A at a) 55% of the chord, b) 70% of the chord, c) 80% of the chord and d) trailing edge.
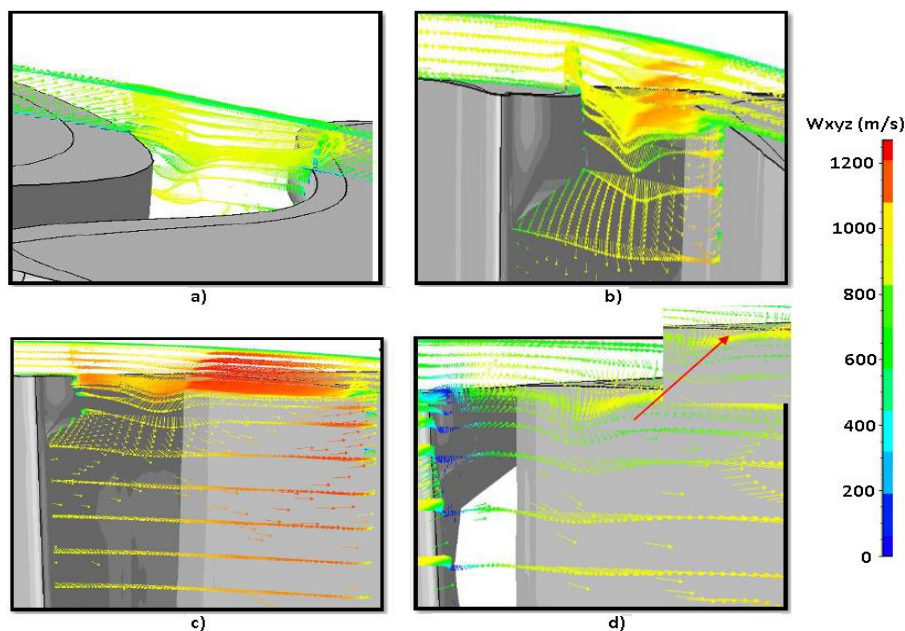

Figure 4. Relative velocity vectors from case B at a) 55% of the chord, b) 70% of the chord, c) 80% of the chord and d) trailing edge.

5.3 Relative velocity streamlines at the rotor tip

As can be observed in Fig 5a, in the base case a separation of flow exists right after the leading edge at the suction surface section, which seems influenced by the streamlines of different velocity that separate at the leading edge and pass from the pressure surface towards the section surface through the tip clearance. These streamlines join themselves with the separated flow and, due to the difference in velocity, form a recirculation, which grows until reaching the trailing edge.
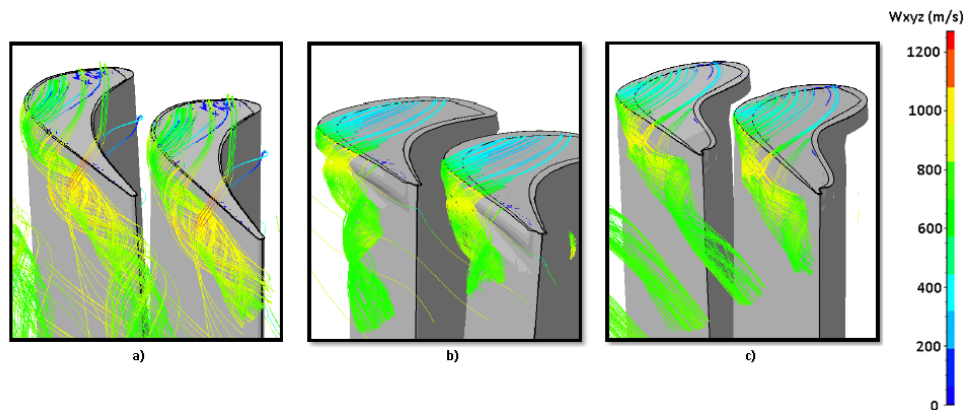

Figure 5. Relative velocity streamlines of a) base case, b) case A and c) case B.

In the case A, a decrease of the leakage vortex can be visualized in Fig. 5b; additionally, there is a decrement in the velocity of the streamlines at the tip clearance and a displacement of the leakage vortex and flow separation zone, which happens due to the winglet on the suction surface. Furthermore, there is a smaller area where the streamlines obtain a higher velocity. It all reflexes on a smaller leakage vortex, which cannot be generated completely in some sections because of the pitch reduction between the blade tips.

Something similar happens in case B, where the leakage vortex moves in the opposite direction to the winglet on the pressure surface, Fig. 5c; however, there is also a decrease of the streamlines velocity at the tip clearance, which causes a smaller difference in velocity, provoking a decrement of the leakage vortices.

5.4 Entropy generation contours at the outlet and blade tip

In Fig. 6a two zones can be identified: the separation bubble at the pressure surface and the flow separation at the suction surface, which causes an increment of the entropy and a wake, where the leakage vortex can be observed. Besides, in Fig. 6b the formation of entropy at the trailing edge can be visualized. The generation of entropy due to the blade geometry and the formation of the leakage vortex can be seen as well.

In case A, the generation of entropy presented a decrement in the leakage vortex intensity, as can be observed in Fig. 7a. Even though in the end it encompassed a bigger area, the generation of the vortex decreases because the recirculation did not get formed completely, increasing the stage performance.

Something similar happened in case B, Fig. 7b, where the decrease of intensity and the shape difference can be visualized. There was no displacement due to the winglet on the pressure surface; however, some characteristics are similar to the ones from case A.
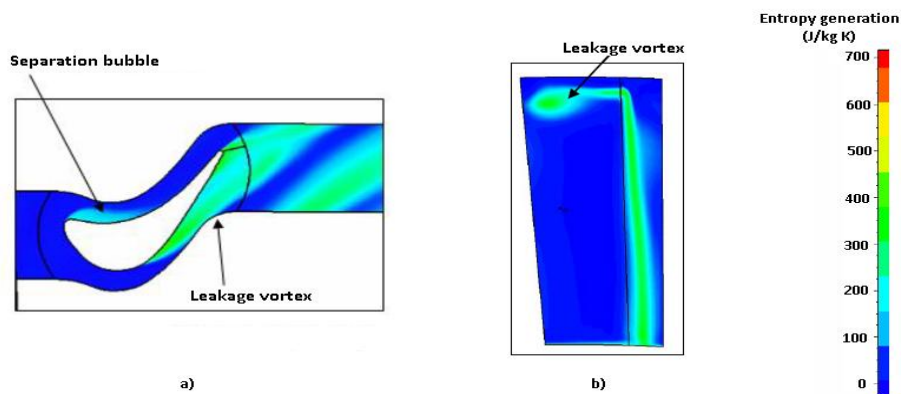

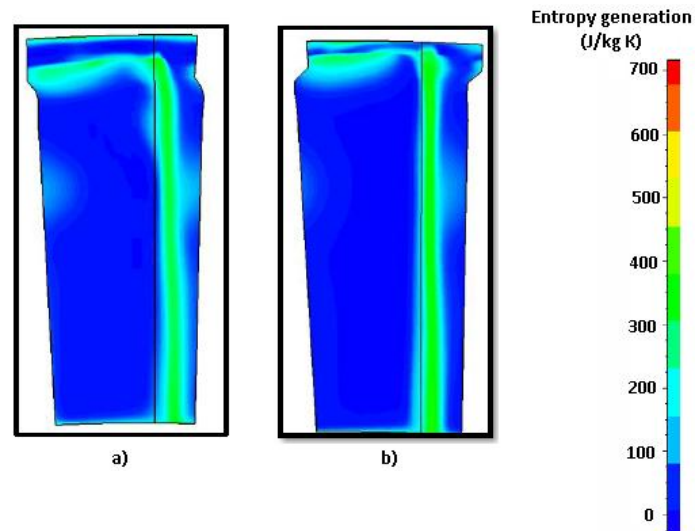**Figure 6.** Entropy contour a) at the blade tip and b) at the outlet

---

Figure 7. Entropy contours at the outlet of a) case A and b) case B.

5.5 Stage efficiency

The final step was to compare the stage efficiency form the three cases, obtaining a value of efficiency equal to 67.52% in the base case, increasing by 10% in the case A and by 7.58% in the case B.

V. Conclusions

On the one side, by obtaining the static pressure contours at the blade tip, a decrement of the wake in the cases A and B was observed. Besides, the implementation of winglets provokes that the leakage vortex displaces to the next blade, avoiding the formation of recirculation, generating a greater efficiency.

On the other side, it could be proved that the generated entropy at the tip clearance is related to the size of the vortex, concluding that as the generation of entropy increases, the stage efficiency decreases.

Then, analyzing all the obtained results it can be concluded that a correct application of winglets can diminish the aerodynamic loses, especially if they are applied at the suction surface.

References

[1]   T.C. Booth, P.R. Dodge, H.K. Hepworth, Rotor-Tip Leakage: Part 1. Basic Methodology, *ASME, 81-GT-71*, 1981.
[2]   N.W. Harvey, K. Ramsden, A computational study of a novel turbine rotor partial shroud, *Journal of Turbomachinery, 123*, 2001, 534-543.
[3]   M. Papa, R.J. Goldstein, F. Gori, Effects of geometry and tip clearance on the mass/heat transfer from a large-scale gas turbine blade, *ASME, Journal of Turbomachinery 125*, 2003, 90-96.
[4]   J.H. Cheon, S.W. Lee, Tip leakage aerodynamics over the cavity squealer tip equipped with coverage winglets in a turbine cascade, *International Journal of Heat and Fluid Flow, 56*, 2015, 60-70.
[5]   A.K. Patel, Research on high work axial gas generator turbine, *SAE, 800618*, 1980.
[6]   D. Dey and C. Camci, Aerodynamic tip desensitization of an axial turbine rotor using tip platform extensions, *ASME, 2001-GT-0484*, 2001.
[7]   S.W. Lee, J.H. Cheon and Q. Zhang, The effect of full coverage winglets on tip leakage aerodynamics over the plane tip in a turbine cascade, *International Journal of Heat and Fluid Flow, 45*, 2014, 23-32.
[8]   Morales da Silva et al, A study of the heat transfer in Winglet and Squealer rotor tip configurations for a non-cooled HPT blade based on CFD calculations, *Turbo Expo*, 2013.
[9]   K. Sarabia, *Caracterización de Álabes de Turbina Axial con Difusores de Vórtices*, Instituto Politécnico Nacinal, Mexico, 2018.
[10]   CFM56 Engine Shop Manual, *General Electric.*
[11]   *User Guide*, AutoGrid5, NUMECA International.
[12]   M. Belmont, C. Tavera, *Análisis numérico de la influencia de la geometría de punta de álabe en la eficiencia termodinámica de una etapa de turbina axial*, Instituto Politécnico Nacional, Mexico, 2016.